processes

Article

Method for Solving the Microwave Heating Temperature Distribution of the TE_{10} Mode

Biao Yang *, **Hongbin Huang, Liexing Zhou and Huaiping Jin**

Faculty of Information Engineering and Automation, Kunming University of Science and Technology, Kunming 650500, China; huanghongbin86@163.com (H.H.); zhouliexing@163.com (L.Z.); jinhuaiping@126.com (H.J.)
* Correspondence: biaoykmust@kust.edu.cn

Abstract: Microwave heating is a process in which the electric, magnetic, and temperature fields are coupled with each other and are characterised by strong non-linearity, high time variability, and infinite dimensionality. This paper proposes a method for predicting the microwave heating temperature distribution of the TE_{10} mode, because the traditional numerical calculation method is not conducive to designing microwave controllers. First, the spatial distribution of the main electromagnetic mode TE_{10} waves in a rectangular waveguide was analysed using the principal mode analysis method. An expression for the transient dissipated power and a heat balance equation with infinite-dimensional characteristics were constructed. Then, the microwave heating model was decomposed into electromagnetic and temperature field submodels. A time discretization approach was used to approximate the transient constant dielectric constant. The heating medium was meshed to solve the electric field strength and transient dissipated power in discrete domains, and the temperature distribution was obtained by substituting this value into the finite-dimensional temperature field submodel. Finally, the validity of the proposed numerical model was verified by comparing the results with the numerical results obtained with the conventional finite element method. The methodology presented in this paper provides a solid basis for designing microwave heating controllers.

Keywords: microwave heating; temperature distribution; numerical models; mesh division; TE_{10} mode

check for updates

Citation: Yang, B.; Huang, H.; Zhou, L.; Jin, H. Method for Solving the Microwave Heating Temperature Distribution of the TE_{10} Mode. *Processes* **2022**, *10*, 1377. https://doi.org/10.3390/pr10071377

Academic Editors: Masoud Soroush and Velislava Lyubenova

Received: 27 May 2022
Accepted: 12 July 2022
Published: 14 July 2022

1. Introduction

In recent years, microwave heating technology has become increasingly prevalent in food processing, metallurgical engineering, materials science, and other fields [1–3]. In the chemical engineering field of multiphase catalytic systems, the use of microwaves provides the possibility of inverting the direction of heat flow, which can facilitate the olefins' reaction on the surface of the catalyst [4]; in the field of construction engineering asphalt pavement maintenance, the use of microwave heating to repair and maintain the pavement can achieve the efficient recycling of asphalt mixture [5]; in the field of materials science metal connection, the use of microwave composite heating to connect large pieces of metal can be free of the constraints of the joint structure and fast and efficient [6]. In contrast to traditional heat radiation, heat convection, and heat conduction methods, microwave heating is selective, fast, and clean. Microwave heating converts electromagnetic energy into heat energy through interactions between electromagnetic waves with polar molecules and charged particles in the heated medium, producing volumetric heat [7–9]. On the one hand, selective heating can be used to selectively heat the material in a mixture; on the other hand, this feature may cause an uneven temperature distribution in the heated material, resulting in hot and cold spots. When the hot spots reach a critical temperature, the heated medium becomes extremely unstable, and the hot spots may drive the temperature to become even higher, resulting in thermal runaway phenomena [10–12]. Therefore, it is important to accurately obtain the temperature domain distribution of the medium within the microwave heating cavity to improve the uniformity of the heating and avoid thermal runaway.

Microwave heating is a process in which the electromagnetic and temperature fields are coupled to each other with strong coupling, nonlinearity, and infinite dimensionality. Together with the inhomogeneous boundary conditions and the temperature dependence of the thermodynamic parameters of the heated medium, it is almost impossible to analyse microwave heating processes using analytical methods. Various studies have proposed different numerical calculation methods for microwave heating processes. Pitchai et al. [13] used the finite-difference time-domain (FDTD) method to construct a three-dimensional electromagnetic thermal model that effectively identified hot and cold spots in food during the heating process. Acevedo et al. [14] used the FDTD method to solve a system of transient Maxwell's equations and constructed a model for the microwave heating of a glass. Jing et al. [15] used the finite-difference time-domain and finite difference method (FDTD-FDM) to numerically simulate the temperature field in microwave-heated polyolefin mixtures, with the FDTD method used to solve the electric field distribution and the FDM used to solve the temperature field distribution. Lou et al. [16] used the finite element method (FEM) to construct a coupled electric—magnetic-thermal model of asphalt heating using microwaves and studied the effects of the heating frequency and power on the electromagnetic and temperature fields within the steel slag asphalt medium. They found that 2.45 GHz was the best frequency to ensure that the electromagnetic and temperature fields had uniform distributions and maximum heating efficiency. Ye et al. [17] used the FEM to model the multiphysics field of a solid sample in a microwave cavity during rotational lifting and combined this model with an implicit function-level set approach to update the dielectric constants in the moving region. Zhou et al. [18] used the FEM to construct a heating model with a conveyor belt inside the heating chamber, and Yi et al. [19] used the FEM to study microwave heating cavities with translational and rotational motion. In recent years, the use of the FEM has become particularly popular in microwave heating studies [20–22]. However, this method usually transforms the heating model into a high-dimensional system of ordinary differential equations during the solution process [23], which is not conducive to the design of microwave heating controllers [24]. With the improvements in computer technology, various commercial softwares (e.g., FDTD Solutions and COMSOL Multiphysics) based on these methods (e.g., FDTD [13,14] and FEM [16–22]) have emerged, which provide a good interactive interface and enable researchers to carry out simulation experiments without knowing the internal mechanism. This will also greatly hinder researchers' understanding of the internal mechanism of microwave heating. It also causes difficulties in extracting the state variables in the reaction process.

Zhong et al. [25] proposed a finite-dimensional ordinary differential equation (ODE) model for microwave heating. They used auxiliary functions to obtain the equivalent homogeneous boundary condition partial differential equation (PDE), derived the characteristic spectrum of the spatial differential operator, and obtained a finite-dimensional ODE model with a modified Galerkin's truncation methods. A one-dimensional heating model of deionised water with a temperature-dependent dielectric constant was obtained using numerical simulations. During microwave heating, the temperature distribution of the medium considerably varied throughout the two-dimensional space, and a one-dimensional heating model may ignore the presence of some hot spots. Zhong et al. [26] analysed microwaves' propagation characteristics in a rectangular medium and the spatial distribution of the primary modes in the medium, derived an explicit expression for the dissipated power in the two-dimensional direction and obtained the global temperature distribution in a medium with a constant dielectric constant with numerical simulations. Treating the dielectric constant as a constant value in the calculation of a two-dimensional heating model is an idealisation that is only suitable for applications in which the accuracy of the model is low. In practical applications, the dielectric constant of a medium depends on the temperature. Therefore, it is of high engineering value to construct a two-dimensional finite-dimensional model of microwave heating with a temperature-dependent dielectric constant.

In this paper, a two-dimensional microwave heating model with a temperature-dependent dielectric constant is constructed. The finite-dimensional calculation method for determining the global temperature distribution of the medium is derived by time discretization, mesh division, and cyclic iteration. This calculation is universally applicable to nonmagnetic media (e.g., potato, silicon carbide (SiC) and Debye media). In Section 2, a conventional microwave heating model is constructed, and the vector distribution characteristics of the TE_{10} mode are analysed using the principal mode analysis method. Based on the distribution characteristics of the TE_{10} mode, the transient dissipated power expressions and heat balance equations are derived in two dimensions. In Section 3, the dielectric constant is considered constant in each time interval by discretizing the heating time. The heating medium is meshed into a finite number of solution domains, and the transient dissipated power in each small solution domain is obtained by solving the electromagnetic field submodel. The transient dissipated power is substituted into the finite-dimensional thermodynamic field submodel to obtain the transient temperature distribution, and the global temperature distribution is calculated using the circular iteration method. In Section 4, the results of the proposed method are compared with those of the FEM calculations from temporal and spatial perspectives. The numerical calculation results demonstrate the validity of the microwave heating model and temperature distribution solution method in the TE_{10} mode.

2. Microwave Heating Temperature Model

2.1. Conventional Microwave Heating Temperature Model

During microwave heating, the coupled oscillating electric and magnetic fields are excited by each other, and their relationship in time can be described by a system of Maxwell equations [27,28]:

$$\begin{cases} \nabla \times H = \dfrac{\partial D}{\partial t} + J_e, J_e = \sigma E, \\ \nabla \times E = -\dfrac{\partial B}{\partial t} - J_m, J_m = \sigma_m H, \\ \nabla \cdot D = \rho_e, \\ \nabla \cdot B = \rho_m, \end{cases} \tag{1}$$

where J_e, J_m, ρ_e, and ρ_m denote the current density, magnetic current density, electric charge density, and magnetic charge density, respectively. σ denotes the electrical conductivity of the medium and σ_m represents the magnetic resistivity of the medium (Ω/m). H, E, D, and B denote the magnetic field vector, electric field vector, electric displacement vector, and magnetic flux density vector, respectively.

The electric field distribution in the microwave reaction chamber can be obtained by solving the Maxwell waveform equation [29,30]:

$$\nabla \times \mu_r^{-1}(\nabla \times E) - k_0^2\left(\varepsilon(T) - \frac{j\sigma}{\omega\varepsilon_0}\right)E = 0, k_0 = \omega\sqrt{\varepsilon_0\mu_0} = \frac{\omega}{c}, \tag{2}$$

where μ_r denotes the relative permeability; $\varepsilon(T)$ denotes the dielectric constant; k_0 denotes the wavenumber in a vacuum; ω denotes the angular frequency of the incident electromagnetic wave; E denotes the incident electric field strength; $\varepsilon_0 = 8.854 \times 10^{-14}$ F/cm denotes the permittivity of the vacuum; $\mu_0 = 4\pi \times 10^{-7}$ H/cm denotes the magnetic permeability of the vacuum; $c = 3.0 \times 10^8$ m $\cdot$ s^{-1} denotes the propagation speed of electromagnetic waves in a vacuum.

During microwave heating, the microscopic heat balance equation within the medium can be described by a typical class of PDEs [31]:

$$\rho C_p \frac{\partial T}{\partial t} = \nabla(\kappa \nabla T) + Q_{abs}(x, y, z, t), \tag{3}$$

where ρ, C_p, and κ denote the density, specific heat capacity, and thermal conductivity of the medium being heated, respectively; T denotes the temperature of the medium at time t; and $Q_{abs}(x, y, z, t)$ is the transient dissipated power, which describes the spatial distribution of the energy absorbed by the medium at time t and can be further determined as [32]:

$$Q_{abs}(x, y, z, t) = \pi f \cdot \varepsilon_0 \cdot \varepsilon''(T) \cdot E \cdot E^* = \pi f \cdot \varepsilon_0 \cdot \varepsilon'(T) \cdot \tan\delta(T) \cdot E \cdot E^*, \tag{4}$$

where f denotes the resonant frequency of the microwave; E and E^* are the electric field strength and complex conjugate of the electric field strength, respectively; $\varepsilon'(T)$ denotes the relative permittivity; $\varepsilon''(T)$ denotes the relative dielectric loss; and $\tan\delta(T) = \varepsilon''(T)/\varepsilon'(T)$ is the loss tangent.

During the heating process, boundary heat convection occurs between the medium and the surrounding air, and the Neumann boundary condition can be obtained according to Newton's law of cooling [33]:

$$\mathbf{n} \cdot \kappa \nabla T = h_c(T - T_\infty), \tag{5}$$

where $\mathbf{n}$ denotes the unit vector pointing outwards at the surface of the medium, and T_∞ denotes the ambient temperature.

2.2. Microwave Heating Temperature Model in TE_{10} Wave Mode

To simplify the model analysis, the following reasonable assumptions are taken into account:

- Assumption 1: The volume of the medium and the mass transferred remain constant during heating.
- Assumption 2: The initial temperature of the medium is uniform.
- Assumption 3: The medium is uniform and isotropic.

During microwave heating, rectangular waveguide cavities and resonant cavities are two common types of heating equipment. The main difference between the two is that the resonant cavity has short-circuiting ends (with near-perfect conductors at the end to enhance electromagnetic resonance) and a circulating water cooling system to protect the magnetrons. In contrast, the rectangular waveguide cavity does not have short-circuiting ends and has an absorber at its end to absorb excess microwaves and protect the magnetron. The walls of rectangular waveguides are typically made of copper, aluminium, or another metallic material. A hollow waveguide transmits only transverse magnetic (TM) and transverse electric (TE) waves and does not transmit transverse electromagnetic (TEM) waves. As the cut-off frequency of the TM wave is higher than that of the TE wave, the analysis is mainly carried out for the TE wave. During microwave heating, the primary mode mainly influences the temperature distribution of the medium. Due to the chosen operating frequency and the waveguide dimensions, the fundamental mode TE_{10} mode is the focus of this analysis.

In a rectangular waveguide, the vector component of the TE_{10} wave can be expressed as [34]:

$$E_y = E_0 \sin\left(\frac{\pi x}{x_0}\right), \tag{6}$$

$$H_x = E_0 \frac{\lambda_0}{\lambda_g} \sqrt{\frac{\varepsilon_0 \varepsilon'(T)}{\mu_0}} \sin\left(\frac{\pi x}{x_0}\right), \tag{7}$$

where E_0 denotes the maximum electric field strength at the centre of the waveguide; x_0 denotes the width of the waveguide; λ_0 denotes the wavelength of the electromagnetic wave in free space, which is defined as:

$$\lambda_0 = \frac{c}{f}, \tag{8}$$

where f denotes the microwave frequency, with 2.45 GHz being a common heating frequency; λ_g denotes the wavelength in the heated material, which can be expressed as:

$$\lambda_g = \frac{\lambda'_g}{\sqrt{1 - \left(\lambda'_g/2x_0\right)^2}}, \lambda'_g = \frac{\lambda_0}{\sqrt{\varepsilon'(T)/2} \cdot \sqrt{\sqrt{1 + \tan^2\delta(T)} + 1}}, \tag{9}$$

According to Poynting's theorem, the power distribution in the heated material can be expressed as [26]:

$$P_{in} = \frac{1}{2} \iint (E_y \times H_x)\, dxdy. \tag{10}$$

In Equation (10), Equations (6) and (7) can ben substitued, and yielding:

$$P_{in} = \frac{1}{4} \sqrt{\frac{\varepsilon'(T)\varepsilon_0}{\mu_0} \left(1 - \left(\frac{\lambda_0}{2x_0}\right)^2\right)} \left(E_0 \sin\left(\frac{\pi x}{x_0}\right)\right)^2 x_0 z_0, \tag{11}$$

where z_0 is the length of the waveguide. The above analysis shows that the TE_{10} wave has only one component and is sinusoidally distributed along the x-axis. The electric field strength at the ends of the waveguide (x = 0, x = x_0) is 0, and the electric field strength reaches its maximum at the centre of the waveguide (x = $x_0/2$), which is exactly half the standing wave. The TE_{10} waves are travelling waves along the z-axis, similar to the propagation process of TEM waves. The electromagnetic field in the TE_{10} mode does not vary in the direction between the broad planes, so a two-dimensional model in the x-z plane is suitable for analysing the electromagnetic field in rectangular waveguides [15]. In the Cartesian coordinate system, considering the temperature distribution of the medium only in the x- and z-axis directions, the transient dissipated power in Equation (4) can be simplified as:

$$Q_{abs}(x,z,t) = Q_{abs}(z,t)\sin^2\left(\frac{\pi x}{x_0}\right) = \pi f \cdot \varepsilon_0 \cdot \varepsilon'(T) \cdot \tan\delta(T) \cdot E_z \cdot E_z^* \cdot \sin^2\left(\frac{\pi x}{x_0}\right), \tag{12}$$

where E_z and E_z^* denote the electric field in the z-axis direction and its conjugate complex, respectively.

The heat balance, in Equation (3), can be reduced to:

$$\rho C_p \frac{\partial T}{\partial t} = \kappa\left(\frac{\partial^2 T}{\partial x^2} + \frac{\partial^2 T}{\partial z^2}\right) + Q_{abs}(x,z,t), \tag{13}$$

By substituting Equation (12) into Equation (13), the heat balance equation can be further expressed as:

$$\rho C_p \frac{\partial T}{\partial t} = \kappa\left(\frac{\partial^2 T}{\partial x^2} + \frac{\partial^2 T}{\partial z^2}\right) + \pi f \cdot \varepsilon_0 \cdot \varepsilon'(T) \cdot \tan\delta(T) \cdot E_z \cdot E_z^* \cdot \sin^2\left(\frac{\pi x}{x_0}\right), \tag{14}$$

The inhomogeneous Neumann boundary condition, Equation (5), can be simplified as:

$$\begin{aligned} \kappa \cdot \frac{\partial T}{\partial x} &= h_c(T - T_a), x = 0, \\ -\kappa \cdot \frac{\partial T}{\partial x} &= h_c(T - T_b), x = x_0, \\ \kappa \cdot \frac{\partial T}{\partial z} &= h_c(T - T_c), z = 0, \\ -\kappa \cdot \frac{\partial T}{\partial z} &= h_c(T - T_d), z = z_0, \end{aligned} \tag{15}$$

The initial temperature conditions are

$$T(x, z, 0) = T_0(x, z), \tag{16}$$

According to Equation (12), the transient dissipated power at $x = 0$ and $x = x_0$ is $Q(0, z, t) = Q(x_0, z, t) = 0$. Thus, no electromagnetic energy is converted to heat energy at the interface in the x-axis direction, the temperature of the heated material is the same as that of the external environment, and there is no thermal convection. Therefore, the inhomogeneous Neumann boundary condition only needs to be considered in the z-axis direction, and Equation (15) can be further simplified:

$$\begin{aligned} \kappa \cdot \frac{\partial T}{\partial z} &= h_c(T - T_c), z = 0, \\ -\kappa \cdot \frac{\partial T}{\partial z} &= h_c(T - T_d), z = z_0, \end{aligned} \tag{17}$$

3. Solving for the Temperature Distribution

By substituting the initial temperature condition Equation (16) and the inhomogeneous Neumann boundary condition Equation (17) into the heat balance Equation (14), the temperature domain distribution of the microwave heating medium can be solved for the TE_{10} mode. However, due to the constraints of the inhomogeneous Neumann boundary conditions, the characteristic spectra of the spatial differential operators $\partial^2 T/\partial x^2$, $\partial^2 T/\partial z^2$ are difficult to extract. In addition, the transient dissipated power varies with the temperature and electric fields and is strongly nonlinear. These problems are difficult to solve using traditional analytical methods.

The microwave heating model can be divided into an electromagnetic field submodel and a thermodynamic field submodel that are linked through the dissipated power term. As the dielectric constant of the material being heated varies with the temperature and frequency, it is difficult to solve the dissipated power. The physical structure of magnetrons in microwave heating equipment makes it difficult to shift the resonant frequency; thus, the solution to the dielectric constant can be simplified by considering only the variation with temperature. To establish the link between the two submodels, the heating time t_{max} was discretized into k time intervals Δt. In each small interval, the current moment's dielectric constant was calculated based on the temperature of the medium at the previous moment and was considered to be constant, and the transient dissipated power was calculated by combining the electric field distributions at that moment.

In this subsection, the time discretization, meshing, and circular iteration methods are utilised to solve the temperature domain distribution of the medium. In Section 3.1, the discrete transient dissipated power is determined by analysing the distribution of the electric field. In Section 3.2, the infinite-dimensional heat balance equation is transformed into a finite-dimensional model. The global temperature distribution is computed by linearly fitting the discrete transient dissipated power obtained in Section 3.1 to the finite-dimensional model and using the temperature at the previous time as the initial value.

3.1. Solving the Electromagnetic Field Submodels

The heating model was meshed, as shown in Figure 1.

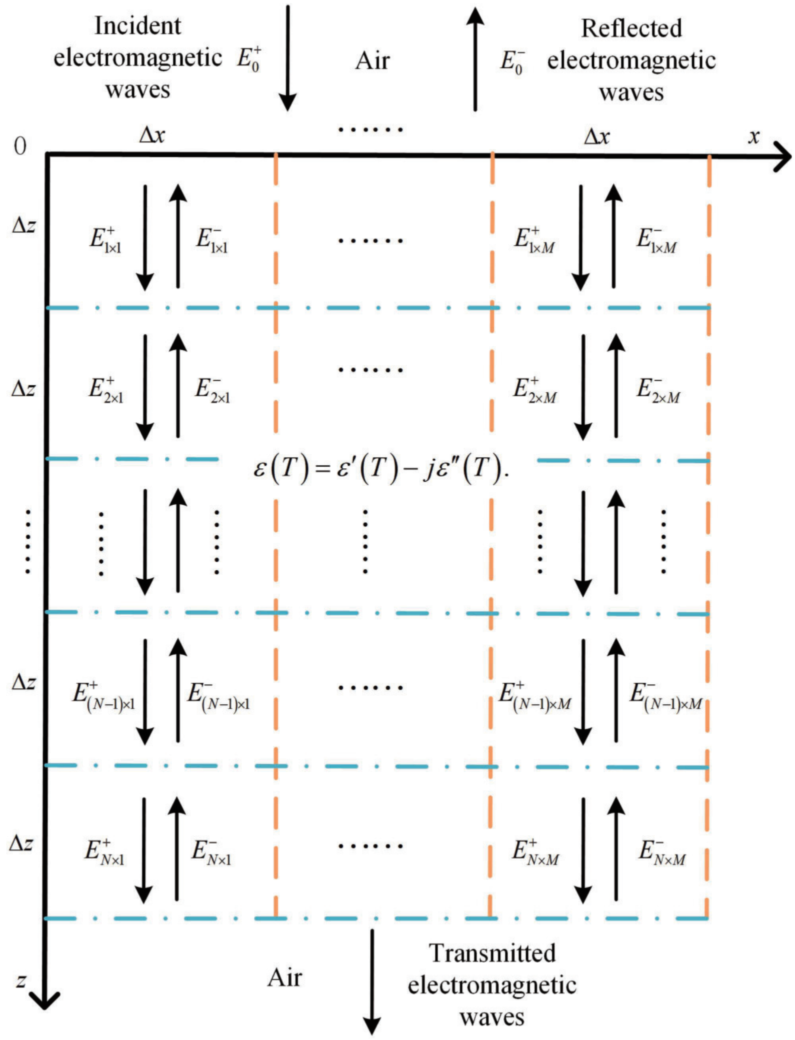

Figure 1. Meshing of the heated material.

The medium was evenly divided into M equal parts along the x-axis, with each interval having a width of Δx. The medium was evenly divided along the z-axis into N equal parts, with each interval having a width of Δz. In each sufficiently small solution domain, the temperature is considered to be uniformly distributed. Based on the distribution characteristics of TE_{10} mode, the electric field distribution in each small solution domain was first calculated in the z-axis direction; then, the sinusoidal distribution in the x-axis direction was computed; finally, the electric field distribution in each small solution domain was determined. To calculate the electric field strength $E_{n\times m}$ in a small solution domain (n rows and m columns), the electric field strength E_n in the nth small solution domain along the z-axis was calculated and substituted into the following equation:

$$E_{n\times m} = E_n \cdot \sin\left(\frac{\pi \cdot \frac{mx_0}{M}}{x_0}\right) = E_n \cdot \sin\left(\frac{\pi \cdot m}{M}\right), n = 1, 2, \ldots, N, m = 1, 2, \ldots, M, \quad (18)$$

Thus, the electric field strength $E_{n\times m}$ of this small solution domain can be calculated. The specific method for determining the electric field strength E_n in the small solution domain in the z-axis direction is as follows.

The curl equations of the Maxwell Equations (1) are:

$$\nabla \times E = -j \cdot 2\pi f \cdot \mu_0 \cdot H, \tag{19}$$

$$\nabla \times H = j \cdot 2\pi f \cdot \varepsilon_0 \cdot E, \tag{20}$$

Equation (19) can be substituted into Equation (20) to obtain the following:

$$\nabla \times \nabla \times E = -j \cdot 2\pi f \cdot \mu_0 \nabla \times H = (2\pi f)^2 \mu_0 \varepsilon_0 E, \tag{21}$$

According to $\nabla \times \nabla \times E = \nabla(\nabla \cdot E) - \nabla^2 E$, Equation (21) can be further expressed as

$$\nabla^2 E + (2\pi f)^2 \mu_0 \varepsilon_0 E = 0, \tag{22}$$

In terms of the electromagnetic boundary conditions, the heated cavity is considered a perfect conductor and the electromagnetic field component inside the conductor is considered zero. The electric field along the tangential direction and the magnetic field along the normal direction at the surface of the heated cavity can be expressed as:

$$E_t = 0, H_t = 0, \tag{23}$$

The electromagnetic boundary condition at the surface–air interface of the heated material is expressed as

$$E_t = E'_t, H_t = H'_t, \tag{24}$$

where E_t and H_t are the electric and magnetic fields on the inner surface of the heated material, respectively, and E'_t and H'_t are the electric and magnetic fields on the outer surface of the heated material, respectively.

When the temperature change in the medium is considered only in the z-axis direction and heat conduction and heat convection in the other directions are neglected, the wave Equation (22) can be further simplified as

$$\frac{d^2 E}{dz^2} + k^2(T)E = 0, \tag{25}$$

where $k(T)$ is the propagation constant, which can be further expressed as

$$k(T) = \frac{2\pi f}{c}\sqrt{\varepsilon(T)} \tag{26}$$

The dielectric constant $\varepsilon(T)$ of the medium can be expressed in complex form as

$$\varepsilon(T) = \varepsilon'(T) - j\varepsilon''(T), \tag{27}$$

Equation (26) can be expanded, yielding

$$k(T) = \alpha(T) + j\beta(T), \tag{28}$$

where $\alpha(T)$ and $\beta(T)$ are the real and imaginary parts of the propagation constant, respectively, which can be further expressed as

$$\alpha(T) = \frac{\omega}{c}\sqrt{\frac{\varepsilon'(T)\left(\sqrt{1+\tan^2\delta(T)}+1\right)}{2}}, \tag{29}$$

$$\beta(T) = \frac{\omega}{c}\sqrt{\frac{\varepsilon'(T)\left(\sqrt{1+\tan^2\delta(T)}-1\right)}{2}}, \tag{30}$$

When the solution domain is sufficiently small, the impedance mismatch within the medium can be neglected. We can determine the electric field strength in the discrete domain (excluding the Nth interval) in the z-axis direction by solving Equation (25)

$$E_n = E_n^+ + E_n^- = E_{n-1}^+ e^{(j\alpha(T_{n-1})-\beta(T_{n-1}))\Delta z} + E_{n+1}^+ e^{(j\alpha(T_n)-\beta(T_n))\Delta z}, n = 1, 2, \ldots, N-1, \tag{31}$$

where E_n^+ and E_n^- are the incident and reflected electric field strengths in the nth solved domain, respectively. The Nth smallest solution domain has an interface between the medium and the air, and the relationship between the incident and reflected electric fields can be obtained by solving for the reflection coefficient. The reflection coefficient between the medium and the air is

$$\Gamma = 1 + \frac{1-\sqrt{\varepsilon(T_N)}}{1+\sqrt{\varepsilon(T_N)}}, \tag{32}$$

By solving Equations (31) and (32), we can obtain the electric field strength E_n in the z-axis direction for any small solution domain. This value can then be substituted into Equation (18) to obtain the electric field strength $E_{n\times m}$ in two dimensions for any small solution domain. The electric field strength and dielectric constant of the small solution domain are substituted into the following equation:

$$\Delta Q_{abs}(n,m,t) = \pi f \cdot \varepsilon_0 \cdot \varepsilon'(T) \cdot \tan\delta(T) \cdot E_{n\times m} \cdot E_{n\times m}^*, \tag{33}$$

Thus, the transient dissipated power value $\Delta Q_{abs}(n,m,t)$ can be calculated for this solution domain.

3.2. Solving the Thermodynamic Field Submodels

The transient dissipated power values $\Delta Q_{abs}(n,m,t)$ for each small solution domain were calculated in the previous subsection; however, the infinite-dimensional thermal equilibrium PDE, as shown in Equation (14), is the primary factor preventing the direct design of the controller. In this subsection, the infinite-dimensional PDE is transformed into a finite-dimensional ODE based on the time discretization and meshing in the previous section, and the temperature distribution is determined.

We can apply reasonable assumptions. When the solution domain in the x-axis direction is sufficiently small, the temperature difference between adjacent solution domains is very small, and heat conduction and heat convection can be ignored. We consider each solution domain (x = 1,2, ... ,M) in the x-axis direction to be independent and determine their temperature distributions in turn. In the calculation of each solution domain, x is considered a constant, and the heat balance Equation (13) can be written as

$$\rho C_p \frac{\partial T}{\partial t} = \kappa \frac{\partial^2 T}{\partial z^2} + Q_{abs}(z,t), \tag{34}$$

While Equation (34) is only the PDE in the z-axis direction, it is still infinite-dimensional. One paper [25] defined the variable

$$k_1 = \frac{\kappa}{\rho C_p}, k_2 = \frac{1}{\rho C_p}, e' = \frac{h_c}{\kappa}(T - T_c), f' = -\frac{h_c}{\kappa}(T - T_d), \tag{35}$$

The eigenvalues and eigenfunctions of the spatial differential operator can be extracted with intermediate variables:

$$\lambda_i = \begin{cases} 0, i = 0, \\ -\left(\frac{i\pi}{z_0}\right)^2, i = 1, 2, \cdots, \infty. \end{cases}$$
$$\phi_i(z) = \begin{cases} \frac{1}{2}, i = 0, \\ \cos\frac{i\pi z}{z_0}, i = 1, 2, \cdots, \infty. \end{cases} \tag{36}$$

The infinite-dimensional PDE can be transformed into an infinite-dimensional ODE, which can then be transformed into a finite-dimensional ODE using Galerkin's truncation method:

$$\dot{\bar{\Theta}}_s(t) = A_s \cdot \bar{\Theta}_s(t) + B_s \cdot u(t) + G_s, \tag{37}$$

$$\Theta_s(z, t) = C_s \cdot \bar{\Theta}_s(t), \tag{38}$$

$$T_s(z, t) = \Theta_s(z, t) + (\frac{f' - e'}{2z_0}z^2 + e'z), \tag{39}$$

where v is the order of the finite dimension,

$$\bar{\Theta}_s(t) = [\bar{\Theta}_0(t), \bar{\Theta}_1(t), \ldots, \bar{\Theta}_v(t)]^{\mathbf{T}},$$

$$A_s = k_1 \cdot diag(\lambda_0, \lambda_1, \ldots, \lambda_v),$$

$$B_s \cdot u(t) = k_2 \frac{2}{z_0} \int_0^{z_0} Q_{abs}(z, t)[\phi_0(z), \ldots, \phi_v(z)]^{\mathbf{T}} dz,$$

$$G_s = k_1 \frac{2}{z_0} \int_0^{z_0} \frac{f' - e'}{z_0} k_1 [\phi_0(z), \ldots, \phi_v(z)]^{\mathbf{T}} dz,$$

$$C_s = [2\phi_0(z), \phi_1(z), \ldots, \phi_v(z)],$$

$$\bar{\Theta}_s(0) = \frac{2}{z_0} \int_0^{z_0} \Theta(z, 0)[\phi_0(z), \ldots, \phi_v(z)]^{\mathbf{T}} dz.$$

Galerkin's truncation is a method for mapping the temperature and energy distributions to a functional global space. The transient dissipated power must be continuously differentiable during the calculation; a linear fit for the transient dissipated power is required in each solution domain. The results of the linear fit are substituted into Equations (37)–(39), and the temperature at the previous time is used as the initial value at the current time to calculate the temperature distribution in each solution domain. The electromagnetic field submodel introduced in Section 3.1 calculates the dielectric constant and electric field distribution based on the temperature distribution at the current moment, then calculates the transient dissipated power. The thermodynamic field submodel introduced in Section 3.2 calculates the temperature distribution based on the transient dissipated power. The model is iterated until the maximum heating time t_{max} is reached.

Algorithm 1 shows the method used to solve the microwave heating temperature distribution based on the circular iterative method.

Algorithm 1: Algorithm for solving the microwave heating temperature distribution of the TE_{10} mode.

1: The thermodynamic and electromagnetic parameters, i.e., the initial temperature $T_0(x,z)$, density ρ, specific heat capacity C_p, thermal conductivity κ, and dielectric constant $\varepsilon(T)$, are initialised.
2: The entire solution space is meshed into a finite number of solution domains.
3: Based on Equations (18), (31) and (32) and the permittivity of each solution domain, the electric field distribution is calculated.
4: Substituting into Equation (33), the transient dissipated power values are obtained for each solved domain $\Delta Q_{abs}(n,m,t)$.
5: Each solution domain Δx in the x-axis direction is considered as a group, and the transient dissipated power in the z-axis direction within the same group are linearly fitted to obtain an explicit expression.
6: The global temperature distribution is calculated by substituting the explicit dissipative power expressions into Equations (37)–(39).
7: The temperature at the current moment is used as a basis to update the dielectric constant of each solution domain.
8: Update $t = t + \Delta t$. If the maximum heating time is reached, end the loop; otherwise, return to Step 3.

4. Results and Analysis

In this subsection, MATLAB numerical simulations are used to validate the proposed method of solving the microwave heating temperature distribution of the TE_{10} mode, and the results are compared with accurate FEM calculation results. The medium being heated is a potato; in this medium, the dielectric constant varies with the temperature, as expressed by [17,35]:

$$\varepsilon(T) = -6.4\times10^{-3}T^2 + 2\times10^{-1}T + 56.8 - j\left(-1\times10^{-4}T^2 - 1.08\times10^{-1}T + 16.1\right), \quad (40)$$

the density ρ = 1050 kg/m^3, the specific heat capacity C_p = 3640 J/(kg · K), and the thermal conductivity κ = 0.648 W/(m · K). A schematic diagram of a rectangular waveguide heating a potato is shown in Figure 2, assuming that the potato fills the entire waveguide.

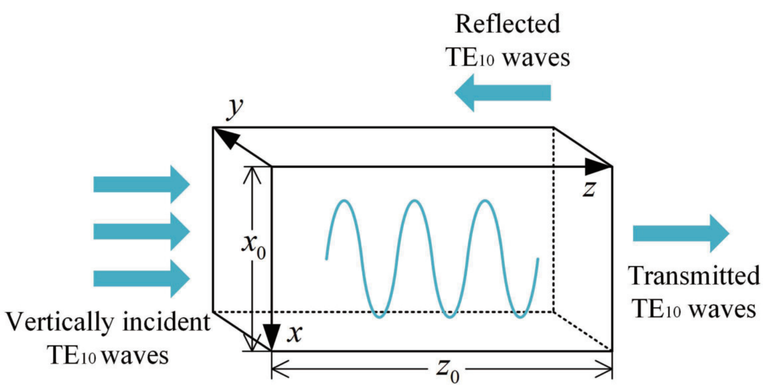

Figure 2. Schematic diagram of a heated potato in a rectangular waveguide.

The feeding microwave frequency is 2.45 GHz. The size of the heated potato is x_0 = 82 mm and z_0 = 80 mm. We consider homogeneous boundary conditions, an initial temperature of 20 °C, a heating time of t_{max} = 10 s, and an initial incident electric field of E_0 = 500 V/cm with zero phase. The discrete transient dissipated power values using a 5th-order polynomial linear fit. The heating time t_{max} is discretised as Δt = 1 s. During spatial meshing, each small solution domain has values of Δx = 0.10 mm in the x-axis direction and Δz = 0.10 mm in the z-axis direction. The method proposed in this paper calculates the temperature distribution inside the potato after 10 s of heating, as shown in Figure 3. The same heating model was constructed using the FEM based COMSOL

Multiphysics simulation software, with a width of 43.2 mm and all other parameters being the same, and the results are shown in Figure 4.

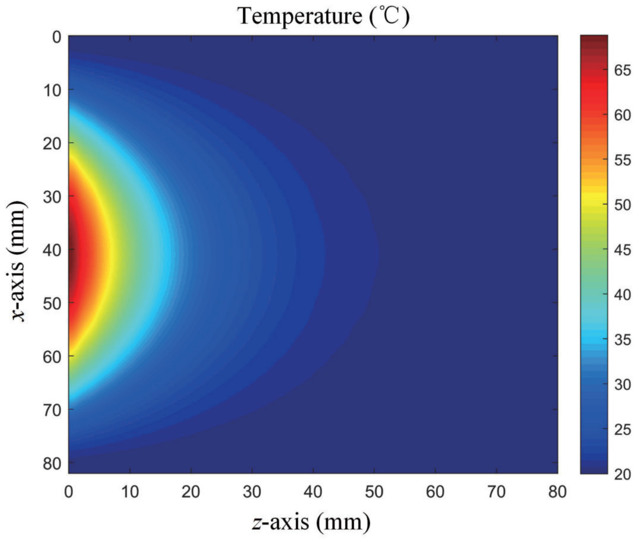

Figure 3. Calculation results of the proposed method.

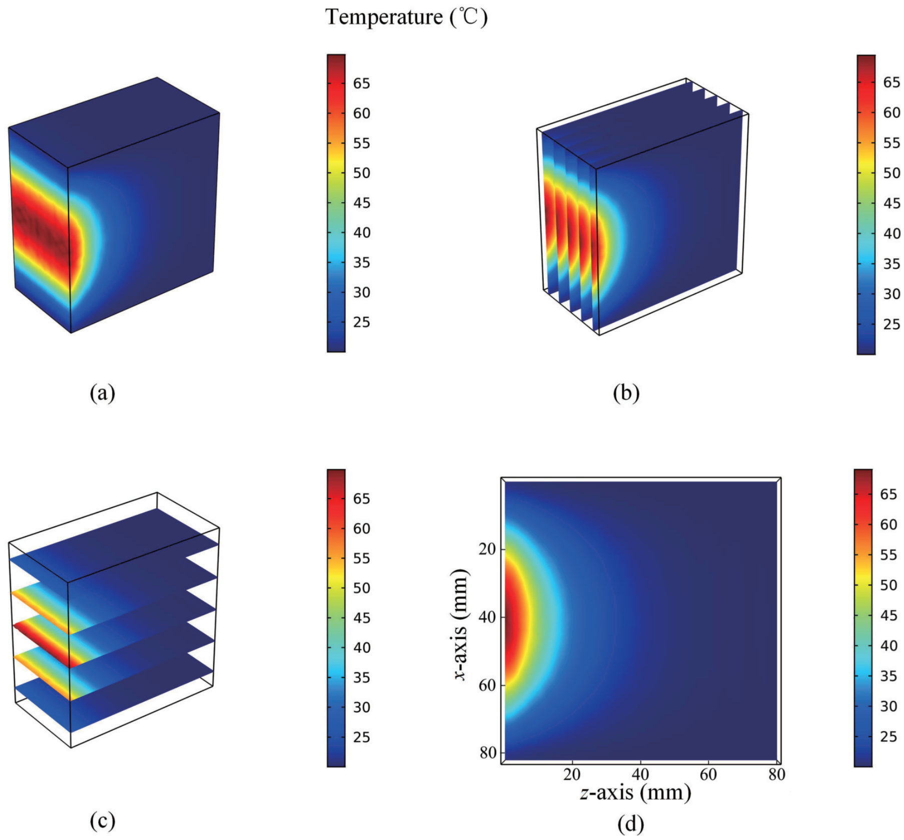

Figure 4. Finite element method (FEM) calculation results. (**a**) Temperature distribution of the material in a rectangular waveguide. (**b**) Temperature distribution in the vertical sections. (**c**) Temperature distribution in the horizontal section. (**d**) Temperature distribution in the central vertical section.

Figures 3 and 4 show that the proposed method is consistent with the FEM calculation results, indicating that the proposed method effectively predicts the temperature domain distribution of the heated medium. The temperature values reach their maximum at x = 41 mm and are distributed along the x-axis in a half-sine period square. The temperature values decay exponentially along the z-axis, which is consistent with Lambert's theorem [26]. When $z \geq 30$ mm, the temperature of the medium is close to room temperature. The temperature distribution at the 10th s for different values of x (i.e., 21, 41, 51, and 71 mm) and z (i.e., 0, 20, 40, and 60 mm) is shown in Figures 5 and 6.

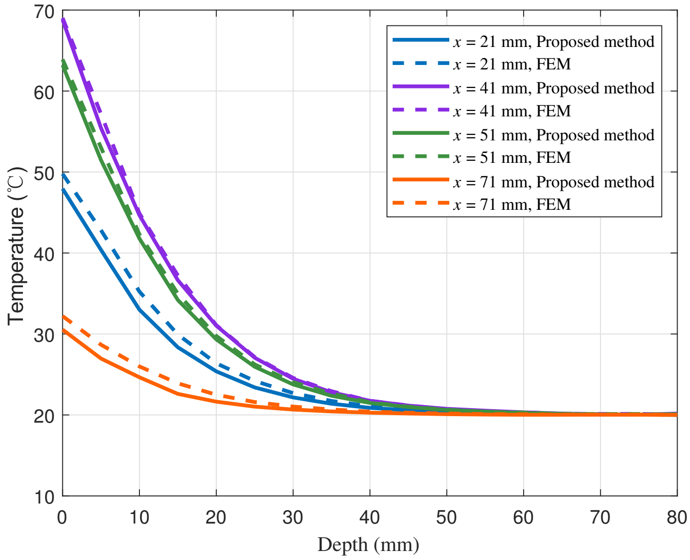

Figure 5. The temperature distribution when x is 21, 41, 51, and 71 mm.

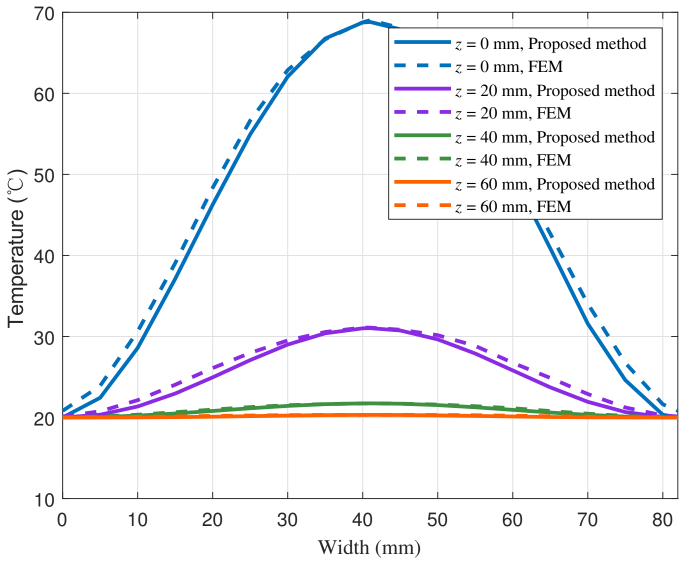

Figure 6. The temperature distribution when z is 0, 20, 40, and 60 mm.

Figures 5 and 6 show that the error between the proposed method and the FEM is smaller at the centre of the x-axis. As the distance from the centre of the x-axis increases, the calculation error increases; however, the proposed method can still approximate the temperature distribution inside the medium. The results show that the proposed model can accurately predict the temperature distribution at the central location and can effectively prevent thermal runaway. The proposed model considers only the steady-state propagation of the TE_{10} mode, neglecting other forms of the electromagnetic field modes. Therefore, in the FEM calculation process, the effect of other electromagnetic field modes leads to a slightly higher value than that obtained with the proposed method.

To further validate the proposed model, the temperature distribution of the whole solution process was analysed. The global temperature distribution at the centre of the x-axis ($x = x_0/2$) is shown in Figures 7 and 8.

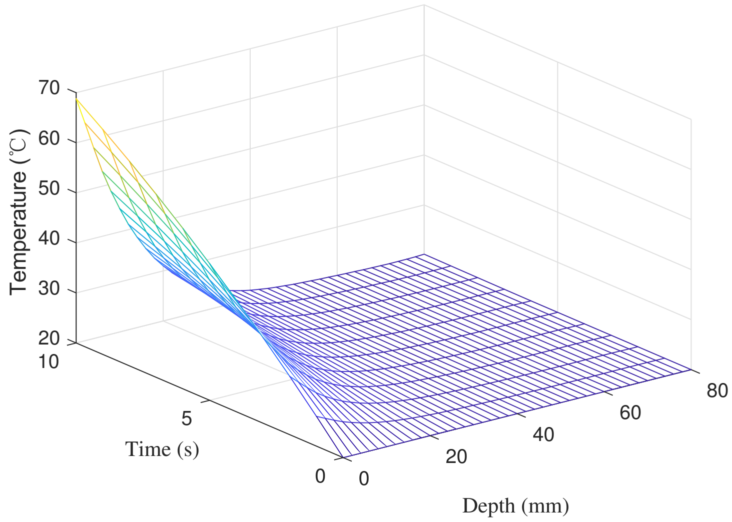

Figure 7. The global temperature distribution calculated by the proposed method at $x = x_0/2$.

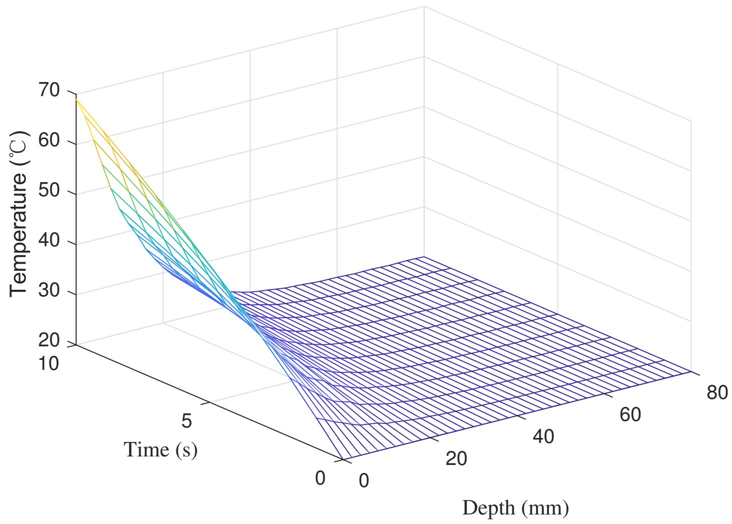

Figure 8. The global temperature distribution calculated by the FEM at $x = x_0/2$.

Figures 7 and 8 show that the results of the two calculation methods are very similar. The rate of the temperature change inside the medium is strongly nonlinear over time. This result occurs because the dielectric constant of the medium changes with the temperature, which, in turn, affects the electric field strength. On the basis of Figures 7 and 8, the numerical results of the two methodologies are further compared. The temperature versus time curves at different depths (z = 0, 20, 40, and 60 mm) are shown in Figure 9. The temperature distributions in the z-axis direction at different moments (t = 2, 4, 6, and 8 s) are shown in Figure 10.

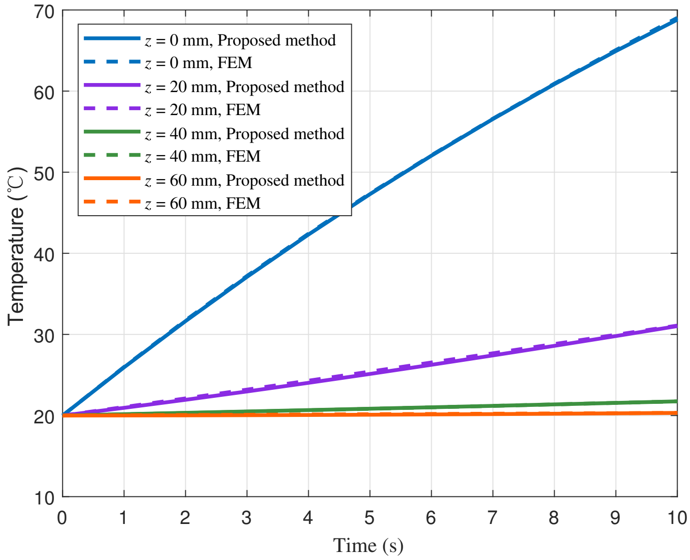

Figure 9. Comparison of the temperature variation results with time at different depths.

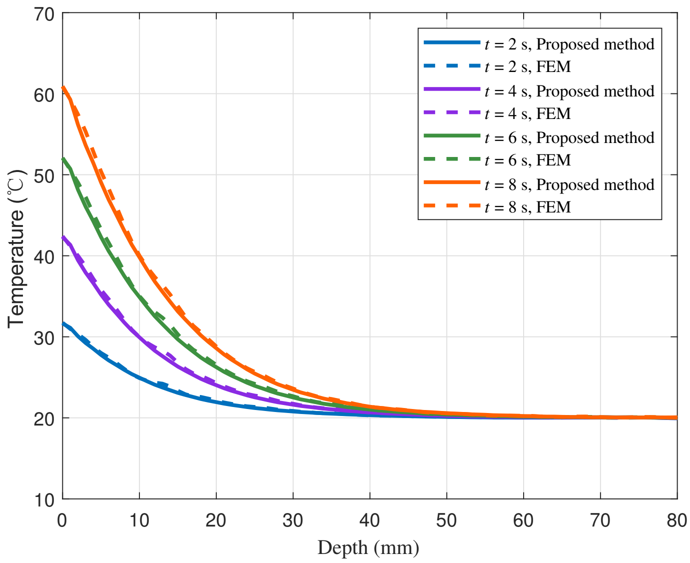

Figure 10. Comparison of the temperature distributions in the z-axis direction at different moments.

The comparison results in Figures 9 and 10 demonstrate that the two numerical calculations are consistent. Although there is a slight error, the global temperature distribution and the rate of change in temperature with time effectively describe the overall microwave heating process. The numerical results demonstrate that the proposed microwave heating model of the TE_{10} mode can be used to effectively predict temperature changes inside the media during heating processes.

5. Conclusions

In this paper, a finite-dimensional microwave heating model of the TE_{10} mode was constructed to approximate the global temperature distribution of a medium with a temperature-dependent dielectric constant. The proposed method overcomes the drawbacks of the conventional microwave heating model of infinite dimensionality and is universally applicable to nonmagnetic media (e.g., potato, SiC and Debye media). The conventional microwave heating model and the vector distribution characteristics of the TE_{10} mode in a rectangular waveguide cavity are analysed, thus simplifying the conventional heating model and constructing a two-dimensional spatial transient dissipated power expression, infinite-dimensional heat balance equation, boundary conditions and initial conditions. For the temperature dependence of the dielectric constant, the heating time is discretized into multiple time domains, and the dielectric constant is considered constant in each time domain. The heating medium is meshed into a finite number of discrete domains. The electric field intensity in each discrete domain is determined by solving Maxwell's equations, and the transient dissipated power is calculated. The transient dissipated power in the discrete domain is linearly fitted to a finite-dimensional thermodynamic field ODE model (obtained by downscaling the traditional PDE model by the modified spectral Galerkin's method) to calculate the transient temperature distribution, and the global temperature distribution of the microwave heating is obtained with a circular iterative method. Finally, the temperature distributions of a material that was heated for 10 s obtained with the proposed finite-dimensional method and the infinite-dimensional FEM are compared, with all parameters being equal. We also compared the results of the solution during the heating process. The comparison results verify the accuracy and validity of the proposed method for predicting the microwave heating temperature distribution of the TE_{10} mode. This method provides a solid basis for preventing thermal runaway and designing microwave heating controllers.

Author Contributions: Conceptualization, B.Y., H.H., L.Z. and H.J.; methodology, B.Y. and H.H.; software, H.H. and H.J.; validation, B.Y. and H.H.; formal analysis, B.Y. and L.Z.; investigation, H.H., L.Z. and H.J.; resources, H.H.; data curation, H.H.; writing—original draft preparation, H.H.; writing—review and editing, H.H.; visualization, H.H.; supervision, B.Y.; project administration, B.Y.; funding acquisition, B.Y. All authors have read and agreed to the published version of the manuscript.

Funding: This research was funded by the National Natural Science Foundation of China (61863020).

Institutional Review Board Statement: Not applicable.

Informed Consent Statement: Not applicable.

Data Availability Statement: All data and models generated or used during the study appear in the submitted article.

Conflicts of Interest: The authors declare no conflict of interest.

References

1. Chandrasekaran, S.; Ramanathan, S.; Basak, T. Microwave food processing-A review. *Food Res. Int.* **2013**, *52*, 243–261. [CrossRef]
2. Omran, M.; Fabritius, T.; Yu, Y.W.; Heikkinen, E.P.; Chen, G.; Kacar, Y. Improving zinc recovery from steelmaking dust by switching from conventional heating to microwave heating. *J. Sustain. Metall.* **2021**, *7*, 15–26. [CrossRef]
3. Tang, L.; Wang, J.; Zhang, B.; Li, C.; Jin, H.H. Remarkable microwave heating performance of MWCNTs/polypropylene composites verified by electromagnetic-thermal coupling experiment and simulation. *Compos. Sci. Technol.* **2022**, *223*, 109428. [CrossRef]
4. Palma, V.; Barba, D.; Cortese, M.; Martino, M.; Renda, S.; Meloni, E. Microwaves and heterogeneous catalysis: a review on selected catalytic processes. *Catalysts* **2020**, *10*, 246. [CrossRef]
5. Luo, W.; Huang, S.Y.; Liu, Y.H.; Peng, H.; Ye, Y. Three-dimensional mesostructure model of coupled electromagnetic and heat transfer for microwave heating on steel slag asphalt mixtures. *Constr. Build. Mater.* **2022**, *330*, 127235. [CrossRef]
6. Tamang, S.; Aravindan, S. Joining of dissimilar metals by microwave hybrid heating: 3D numerical simulation and experiment. *Int. J. Therm. Sci.* **2021**, *172*, 107281. [CrossRef]
7. Bhattacharya, M.; Basak, T. A review on the susceptor assisted microwave processing of materials. *Energy* **2016**, *97*, 306–338. [CrossRef]
8. Shang, X.B.; Zhai, D.; Chong, C.Y.; Zhang, F.C.; Wei, C.; Chen, J.R.; Liu, M.H.; Peng, J.H. Electromagnetic waves transmission performance of alumina refractory ceramics in 2.45 GHz microwave heating. *Ceram. Int.* **2019**, *45*, 23493–23500. [CrossRef]
9. Dinani, S.T.; Feldmann, E.; Kulozik, U. Effect of heating by solid-state microwave technology at fixed frequencies or by frequency sweep loops on heating profiles in model food samples. *Food Bioprod. Process.* **2021**, *127*, 328–337. [CrossRef]
10. Yakata, R.; Sonobe, S.; Asakuma, Y.; Hyde, A.; Phan, C.; Sen, T.K. Characterization of heating behaviour of a microwave reactor during mixing. *Therm. Sci. Eng. Prog.* **2022**, *29*, 101206. [CrossRef]
11. Wang, C.R.; Yao, W.; Zhu, H.C.; Yang, Y.; Yan, L.P. Uniform and highly efficient microwave heating based on dual-port phase-difference-shifting method. *Int. J. Microw. Comput. Eng.* **2021**, *31*, e22784. [CrossRef]

12. Su, T.Y.; Zhang, W.Q.; Zhang, Z.J.; Wang, X.W.; Zhang, S.W. Energy utilization and heating uniformity of multiple specimens heated in a domestic microwave oven. *Food Bioprod. Process.* **2022**, *132*, 35–51. [CrossRef]
13. Pitchai, K.; Birla, S.L.; Subbiah, J.; Jones, D.; Thippareddi, H. Coupled electromagnetic and heat transfer model for microwave heating in domestic ovens. *J. Food Eng.* **2012**, *112*, 100–111. [CrossRef]
14. Acevedo, L.; Uson, S.; Uche, J. Numerical study of cullet glass subjected to microwave heating and SiC susceptor effects. Part I: Combined electric and thermal model. *Energ. Convers. Manag.* **2015**, *97*, 439–457. [CrossRef]
15. Jing, X.D.; Wen, H.; Xu, Z.H. Temperature field simulation of polyolefin-absorber mixture by FDTD-FDM model during microwave heating. *Chin. J. Chem. Eng.* **2020**, *28*, 2900–2917. [CrossRef]
16. Lou, B.W.; Sha, A.M.; Barbieri, D.M.; Liu, Z.Z.; Zhang, F. Microwave heating properties of steel slag asphalt mixture using a coupled electromagnetic and heat transfer model. *Constr. Build. Mater.* **2021**, *291*, 123248. [CrossRef]
17. Ye, J.H.; Xia, Y.; Yi, Q.Y.; Zhu, H.C.; Yang, Y.; Huang, K.M.; Shi, K.B. Multiphysics modeling of microwave heating of solid samples in rotary lifting motion in a rectangular multi-mode cavity. *Innov. Food Sci. Emerg.* **2021**, *73*, 102767. [CrossRef]
18. Zhou, J.; Yang, X.Q.; Chu, Y.; Li, X.; Yuan, J.P. A novel algorithm approach for rapid simulated microwave heating of food moving on a conveyor belt. *J. Food Eng.* **2020**, *282*, 110029. [CrossRef]
19. Yi, Q.Y.; Lan, J.Q.; Ye, J.H.; Zhu, H.C.; Yang, Y.; Wu, Y.Y.; Huang, K.M. A simulation method of coupled model for a microwave heating process with multiple moving elements. *Chem. Eng. Sci.* **2021**, *231*, 116339. [CrossRef]
20. Ye, J.H.; Lan, J.Q.; Xia, Y.; Yang, Y.; Zhu, H.C.; Huang, K.M. An approach for simulating the microwave heating process with a slow-rotating sample and a fast-rotating mode stirrer. *Int. J. Heat Mass Tran.* **2019**, *140*, 440–452. [CrossRef]
21. He, J.L.; Yang, Y.; Zhu, H.C.; Li, K.; Yao, W.; Huang, K.M. Microwave heating based on two rotary waveguides to improve efficiency and uniformity by gradient descent method. *Appl. Therm. Eng.* **2020**, *178*, 115594. [CrossRef]
22. Teimoori, K.; Cooper, R. Multiphysics study of microwave irradiation effects on rock breakage system. *Int. J. Rock Mech. Min.* **2021**, *140*, 104586. [CrossRef]
23. Upadhyay, S.; Rai, K.N. A new iterative least square Chebyshev wavelet Galerkin FEM applied to dual phase lag model on microwave drying of foods. *Int. J. Therm. Sci.* **2019**, *139*, 217–231. [CrossRef]
24. Zhong, J.Q.; Liang, S.; Xiong, Q.Y. Improved receding horizon H-infinity temperature spectrum tracking control for Debye media in microwave heating process. *J. Process Contr.* **2018**, *71*, 14–24. [CrossRef]
25. Zhong, J.Q.; Liang, S.; Yuan, Y.P.; Xiong, Q.Y. Coupled electromagnetic and heat transfer ODE model for microwave heating with temperature-dependent permittivity. *IEEE T. Microw. Theory* **2016**, *64*, 2467–2477. [CrossRef]
26. Zhong, J.Q.; Liang, S.; Xiong, Q.Y.; Yuan, Y.P.; Zeng, C. Approximate microwave heating models for global temperature profile in rectangular medium with TE10 mode. *J. Therm. Anal. Calorim.* **2015**, *122*, 487–495. [CrossRef]
27. Meng, Q.; Lan, J.Q.; Hong, T.; Zhu, H.C. Effect of the rotating metal patch on microwave heating uniformity. *J. Microw. Power Electromagn. Energy* **2018**, *52*, 94–108. [CrossRef]
28. Xiong, G.C.; Zhu, H.C.; Huang, K.M.; Yang, Y.; Fan, Z.P.; Ye, J.H. The impact of pins on dual-port microwave heating uniformity and efficiency with dual frequency. *J. Microw. Power Electromagn. Energy* **2020**, *54*, 83–98. [CrossRef]
29. Yang, B.; Sun, J.; Li, W.; Peng, J.H.; Li, Y.L.; Luo, H.L.; Guo, S.H.; Zhang, Z.M.; Su, H.Z.; Shi, Y.M. Numerical modeling dynamic process of multi-feed microwave heating of industrial solution media. *J. Cent. South Univ.* **2016**, *23*, 3192–3203. [CrossRef]
30. Halim, S.A.; Swithenbank, J. Simulation study of parameters influencing microwave heating of biomass. *J. Energy Inst.* **2019**, *92*, 1191–1212. [CrossRef]
31. Llave, Y.; Kambayashi, D.; Fukuoka, M.; Sakai, N. Power absorption analysis of two-component materials during microwave thawing and heating: Experimental and computer simulation. *Innov. Food Sci. Emerg.* **2020**, *66*, 102479. [CrossRef]
32. Liao, Y.H.; Wu, Z.Y.; Feng, X.P. Characteristics of heating process in microwave applicators with elements in periodic motion. *Int. J. Microw. Comput. Eng.* **2019**, *29*, e21641. [CrossRef]
33. Zhang, M.; Jia, X.B.; Tang, Z.X.; Zeng, Y.X.; Wang, X.J.; Liu, Y.; Ling, Y.Q. A Fast and Accurate Method for Computing the Microwave Heating of Moving Objects. *Appl. Sci.* **2020**, *10*, 2985. [CrossRef]
34. Klinbun, W.; Rattanadecho, P.; Pakdee, W. Microwave heating of saturated packed bed using a rectangular waveguide (TE10 mode): Influence of particle size, sample dimension, frequency, and placement inside the guide. *Int. J. Heat Mass Tran.* **2011**, *54*, 1763–1774. [CrossRef]
35. Zhu, H.C.; He, J.B.; Hong, T.; Yang, Q.Z.; Wu, Y.; Yang, Y.; Huang K.M. A rotary radiation structure for microwave heating uniformity improvement. *Appl. Therm. Eng.* **2018**, *141*, 648–658. [CrossRef]